Steady-state perturbative theory for nonlinear circuits

Steady-state perturbative theory for nonlinear circuits

Harish S Bhat[1] **, Wooram Lee**[2] **, Georgios N Lilis**[2] **and Ehsan Afshari**[2]

[1] School of Natural Sciences, University of California, Merced, Merced, CA 95343, USA
[2] Electrical and Computer Engineering, Cornell University, Ithaca, NY 14853, USA

E-mail: hbhat@ucmerced.edu

Abstract

We study the steady-state behavior of a damped, driven nonlinear LRC oscillator, where the nonlinearity arises due to voltage-dependent capacitance. The driving or input signal is assumed to be a pure tone. Using an iterative, perturbative solution technique combined with an energy conservation argument, we show that the oscillator transfers energy from the fundamental to higher harmonics. We determine a series expansion of the two-norm of the steady-state output signal and show that in a large region of parameter space, the two-norm depends superlinearly on the input amplitude. We also use the two-norm calculation to devise a performance goal that the infinity-norm of the steady-state output signal should satisfy, in order for the nonlinear system to have a genuine boost over the corresponding linear system. Taken together, these results are a step toward the automatic design of nonlinear systems that have an optimal boost over corresponding linear systems.

PACS numbers: 05.45.Yv, 84.30.Ng, 63.20.Ry

1. Introduction

Recently, two-dimensional lattices consisting of inductors and voltage-dependent capacitors have been proposed for high-frequency analog signal shaping applications [ABHM06, BA08, LPL+10]. A schematic diagram for a typical lattice is shown in figure 1. The voltage dependence of the capacitors causes nonlinear propagation of voltage/current in the lattice. Unlike earlier studies that focused on using bulk-scale versions of these lattices to generate solitons [OPS80, Ste81, Ste83] modern applications involve fabricating these lattices on chip using CMOS processes, in order to generate and process microwave signals in the analog domain. The advantage of using inductor–capacitor lattices is that they consist of passive devices, with higher cutoff frequencies than active devices (such as transistors) on the same process.

In order to exploit the natural dynamics of these lattices for applications, we must have a detailed understanding of their qualitative and quantitative dynamics. In our earlier work
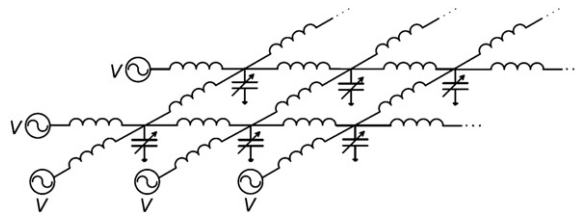
Figure 1. Typical two-dimensional lattice (or network) of inductors and voltage-dependent capacitors.
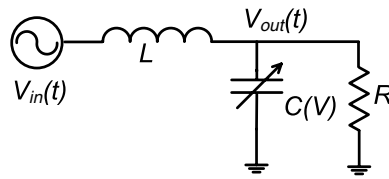
Figure 2. Damped, driven nonlinear *LRC* oscillator.

[BA08, LPL+10], we established that when the left and bottom boundaries of the two-dimensional lattice shown in figure 1 are driven by constant amplitude, in-phase sinusoidal sources, the lattice pushes energy into higher harmonics, yielding output signals with larger peak-to-peak amplitudes and higher frequency content than the sources. One of the strategies we used was to consider a much smaller problem, a single nonlinear *LC* (inductor–capacitor) oscillator connected to a resistive load *R* that stands in for the rest of the lattice, as shown in figure 2. Using numerical methods, we established that the amplitude of the steady-state output signal depends nonlinearly on the amplitude of the driving signal. We refer to this as amplitude boosting.

In this work, our goal is to give an analytical explanation of how nonlinearity can boost the L^2 and L^∞ norms of the steady-state output of the nonlinear system, relative to the steady-state output of the corresponding linear system. In section 2, we derive a perturbative steady-state solution in the case where the driving function consists of a pure tone, i.e. a trigonometric function with fixed amplitude oscillating at a single frequency. What we find is that the natural behavior of the oscillator is to push energy from the fundamental frequency into higher harmonics. Next, we use the steady-state solution together with an energy conservation argument to relate the L^2 norm of the output signal $V_{\text{out}}(t)$ to the amplitude of a pure tone input signal $V_{\text{in}}(t)$, and to thereby derive a lower bound on the L^∞ norm of the output signal. This is carried out in section 3.

Until this point, our derivations are general and do not depend on specific choices of the parameters for circuit inductance, capacitance and resistance. In sections 3.3 and 3.4, we show that for practical choices of these circuit parameters, the L^2 and L^∞ norms of V_{out} depend nonlinearly and in fact superlinearly on the amplitude of V_{in}. This result helps to explain prior numerical and experimental observations where doubling the input amplitude caused the output amplitude to increase by more than a factor of 2.

It would be impossible to survey all prior studies on damped, driven nonlinear oscillators. There has been a tremendous amount of work in this area, much of which has been comprehensively surveyed elsewhere [NM79, VMM+96]. Unlike the work on, for example,

the damped, driven Duffing oscillator, the purpose of our work is not to demonstrate chaos. Many nonlinear chaotic circuits have been discussed in the literature, including a circuit known as the series nonlinear LRC oscillator, with all three components arranged in series, unlike ours. In the parameter regimes we consider, and in a neighborhood of the initial conditions $(V(0), \dot{V}(0)) = (0, 0)$, the equations under study do not display sensitive dependence on initial conditions [BA08]. We make further remarks on the difference between our nonlinear oscillator equation and more standard nonlinear oscillator equations in section 2.

2. Steady-state solution

Consider the circuit shown in figure 2. Let $V(t) = V_{\text{out}}(t)$, and let $Q(t)$ denote the charge stored in the capacitor at time t. Using Kirchhoff's laws of voltage and current, we write the following equations:

$$L\frac{dI}{dt} = V_{\text{in}}(t) - V, \tag{1a}$$

$$\frac{dQ}{dt} = I - \frac{V}{R}. \tag{1b}$$

The charge is related to the voltage via

$$Q(V) = \int_0^V C(v)\,dv, \tag{2}$$

which implies that (1b) is equivalent to

$$\frac{dQ}{dt} = C(V)\frac{dV}{dt} = I - \frac{V}{R}. \tag{3}$$

Differentiating (3) with respect to t and using (1a), we obtain

$$\frac{d}{dt}\left[C(V)\frac{dV}{dt}\right] + \frac{1}{R}\frac{dV}{dt} + \frac{1}{L}V = \frac{1}{L}V_{\text{in}}(t). \tag{4}$$

We make the following assumptions.

- R and L are positive constants.
- $C(V)$ is weakly dependent on V, i.e.

$$C(v) = C_0 + \varepsilon C_1 v, \tag{5}$$

  where C_0 and C_1 are constants and $\varepsilon < 1$.
- The input function is a trigonometric function oscillating at one, fixed frequency.

At this point, it is important to understand that with the specific form of $C(v)$ considered here, the second-order equation (4) becomes

$$C_0\frac{d^2V}{dt^2} + \varepsilon C_1\left(\frac{dV}{dt}\right)^2 + \varepsilon C_1 V\frac{d^2V}{dt^2} + \frac{1}{R}\frac{dV}{dt} + \frac{1}{L}V = \frac{1}{L}V_{\text{in}}(t). \tag{6}$$

Writing out all the terms allows us to compare our approach with another approach that is more commonly used [BW06, BW07], which is to write a second-order equation for the charge Q. To do this, we note that (5) and (2) imply $Q(V) = C_0 V + \varepsilon C_1 V^2/2$, so

$$V = \frac{1}{C_0}Q - \varepsilon\frac{C_1}{2C_0^3}Q^2 + O(\varepsilon^2).$$

Then differentiating (1*b*) with respect to *t* yields

$$\frac{d^2 Q}{dt^2} = \frac{dI}{dt} - \frac{1}{R}\frac{dV}{dt} \tag{7}$$

$$= \frac{1}{L}V_{\text{in}}(t) - \frac{1}{L}V - \frac{1}{R}\frac{dV}{dt} \tag{8}$$

$$= \frac{1}{L}V_{\text{in}}(t) - \frac{1}{LC_0}Q + \varepsilon\frac{C_1}{2LC_0^3}Q^2 - \frac{1}{RC_0}\frac{dQ}{dt} + \varepsilon\frac{C_1}{RC_0^3}Q\frac{dQ}{dt} + O(\varepsilon^2). \tag{9}$$

Dropping the $O(\varepsilon^2)$ remainder term and assembling the non-forcing terms on the left-hand side, we obtain the second-order equation

$$\frac{d^2 Q}{dt^2} + \frac{1}{RC_0}\frac{dQ}{dt} - \varepsilon\frac{C_1}{RC_0^3}Q\frac{dQ}{dt} + \frac{1}{LC_0}Q - \varepsilon\frac{C_1}{2LC_0^3}Q^2 = \frac{1}{L}V_{\text{in}}(t). \tag{10}$$

In the context of nonlinear oscillation theory, the form of (10) is more similar to equations discussed previously [NM79, Hay85, VMM+96], where the highest order derivative appears linearly (and not nonlinearly) in the equation, unlike in (6). In fact, the free oscillations of (10), with $V_{\text{in}}(t) \equiv 0$, have been analyzed in recent work on quadratic nonlinear oscillators [Mic04, Hu06].

It is important to keep in mind that $O(\varepsilon^2)$ terms were dropped when passing from (1) to (10). Our derivation and results do not involve dropping any terms, and we will be interested in analyzing the perturbative solutions of (6) at *all* orders of ε. Even if full solutions to the damped, driven nonlinear oscillator equation (10) are available at all orders of ε, we have no reason to expect these solutions to agree with solutions of (6) beyond the first order of ε.

We return to the analysis of (4). Under the assumptions made above, we wish to show that (i) the effect of nonlinearity is to excite higher harmonics, and that (ii) nonlinearity does not cause a shift in the oscillation frequency—the period of the output signal $V(t)$ equals the period of the input signal $V_{\text{in}}(t)$. We start by writing

$$V(t) \sim \sum_{k=0}^{\infty} \varepsilon^k w_k(t). \tag{11}$$

Substituting this into (4), using the Cauchy product of infinite series, and separating out the $k = 0$ equation lead to the sequence of problems

$$k = 0: \quad \mathcal{L}w_0(t) = \frac{1}{L}V_{\text{in}}(t), \tag{12}$$

$$k \geqslant 1: \quad \mathcal{L}w_k(t) = -C_1\frac{d}{dt}\sum_{n=0}^{k-1} w_n(t)\frac{d}{dt}w_{k-1-n}(t), \tag{13}$$

where $\mathcal{L}$ is the operator

$$\mathcal{L} = C_0\frac{d^2}{dt^2} + \frac{1}{R}\frac{d}{dt} + \frac{1}{L}.$$

In the previous work [BA08], we analyzed (4) with the input function

$$V_{\text{in}}(t) = A\sin 2\pi\omega t \tag{14}$$

using a very concrete version of the above approach—we explicitly calculated the four terms w_0, w_1, w_2 and w_3. Also in the previous work [LPL+10], we found the frequency response of the system by taking the Fourier transform of (4) and then using a perturbative expansion in

the frequency domain. The results included a sequence of equations involving convolutions similar to that appearing on the right-hand side of (13).

We proceed with a few lemmas that will lead us to understand amplitude boosting in section 3. In what follows, we use $\hat{f}(\nu)$ to denote the Fourier transform of $f(t)$:

$$\hat{f}(\nu) = \int_{-\infty}^{\infty} f(t)\, e^{-2\pi i \nu t}\, dt. \tag{15}$$

Then the inverse Fourier transform is written as

$$f(t) = \int_{-\infty}^{\infty} \hat{f}(\nu)\, e^{2\pi i \nu t}\, d\nu. \tag{16}$$

We shall also use

$$F(s) := \int_{t=0}^{\infty} e^{-st} F(t)\, dt$$

to denote the Laplace transform of $F(t)$—in other words, if we write a function of s, it is understood that this is the Laplace transform of the corresponding function of t.

Lemma 1 simply records the steady-state solution of a damped, driven linear oscillator, regardless of the initial condition. In what follows, we use $H(t)$ to denote the Heaviside step function.

Lemma 1. *Suppose we have an input function $V_{\rm in}(t) = \sum_{m=1}^{M} \beta_m\, e^{2\pi i \alpha_m t}$, where $\alpha_m \in \mathbb{R}$ and $\beta_m \in \mathbb{C}$. Then, for any initial conditions $(V(0), \dot{V}(0))$, the steady-state solution of the linear system*

$$\mathcal{L}V(t) = L^{-1} V_{\rm in}(t) H(t) \tag{17}$$

is given by

$$V_{\rm steady}(t) = \sum_{m=1}^{M} e^{2\pi i \alpha_m t} \frac{\beta_m L^{-1}}{C_0 (2\pi i \alpha_m)^2 + R^{-1}(2\pi i \alpha_m) + L^{-1}}. \tag{18}$$

Proof.   Consider the initial-value problem where $V(0)$ and $\dot{V}(0)$ are given, and where it is assumed that $V(t) = V(t)H(t)$, or in other words, $V(t) \equiv 0$ for $t < 0$. Applying the Laplace transform to both sides of the linear system, we find that

$$V(s) = \underbrace{\frac{L^{-1} V_{\rm in}(s)}{C_0 s^2 + R^{-1} s + L^{-1}}}_{V_S(s)} + \underbrace{\frac{C_0(s V(0) + \dot{V}(0)) + R^{-1} V(0)}{C_0 s^2 + R^{-1} s + L^{-1}}}_{V_T(s)}.$$

The term $V_T(s)$ is of the form $P(s)/Q(s)$ where the degree of the polynomial P is strictly less than the degree of the polynomial Q. Moreover, the roots of $Q(s) = C_0 s^2 + R^{-1} s + L^{-1}$ are located at

$$s_{\pm} = -\tfrac{1}{2} R^{-1} C_0^{-1} \pm \sqrt{\tfrac{1}{4} R^{-2} C_0^{-2} - L^{-1} C_0^{-1}}.$$

Since R, C_0, and L are always positive, both roots of $Q(s)$ always have strictly negative real part. Trivially, $\lim_{s \to 0}[s V_T(s)] = 0$, and since the hypotheses of the final value theorem are satisfied, we know that $\lim_{t \to \infty} V_T(t) = 0$—this holds regardless of the initial conditions $V(0)$ and $\dot{V}(0)$. Since V_T decays to zero for large t, we focus our attention on V_S. We first write

$$V_{\rm in}(s) = \sum_{m=1}^{M} \frac{\beta_m}{s - 2\pi i \alpha_m}.$$

Hence,

$$V_S(s) = \sum_{m=1}^{M} \frac{\beta_m L^{-1}}{(s - 2\pi i\alpha_m)(C_0 s^2 + R^{-1}s + L^{-1})}.$$

Inverting the Laplace transform on the right-hand side is simple. At the end of this derivation, we will treat the case where $Q(s)$ has a double root at $s_* = -(1/2)R^{-1}C_0^{-1}$; for now, assume that $s_+ \neq s_-$. Then taking the inverse Laplace transform yields

$$V_S(t) = \sum_{m=1}^{M} e^{2\pi i\alpha_m t} \frac{\beta_m L^{-1}}{C_0(2\pi i\alpha_m)^2 + R^{-1}(2\pi i\alpha_m) + L^{-1}}$$
$$+ \sum_{m=1}^{M} e^{s_+ t} \frac{\beta_m L^{-1}}{(s_+ - 2\pi i\alpha_m)(s_+ - s_-)C_0} + \sum_{m=1}^{M} e^{s_- t} \frac{\beta_m L^{-1}}{(s_- - 2\pi i\alpha_m)(s_- - s_+)C_0}. \quad (19)$$

Since the real parts of $s_\pm$ are strictly negative, the terms involving $e^{s_\pm t}$ decay to zero as $t \to \infty$. Therefore, we have proven

$$\lim_{t \to \infty} |V(t) - V_{\text{steady}}(t)| = 0, \quad (20)$$

as desired.

If $R = (1/2)\sqrt{L/C_0}$, then the polynomial $Q(s)$ has a double root at $s_* = -(1/2)R^{-1}C_0^{-1}$. In this case, instead of (19), the inverse Laplace transform of $V_S(s)$ will give

$$V_S(t) = \sum_{m=1}^{M} e^{2\pi i\alpha_m t} \frac{\beta_m L^{-1}}{C_0(2\pi i\alpha_m)^2 + R^{-1}(2\pi i\alpha_m) + L^{-1}} + \frac{L^{-1}}{2C_0} \sum_{m=1}^{M} \frac{d}{ds}\bigg|_{s=s_*} \frac{\beta_m e^{st}}{s - 2\pi i\alpha_m}. \quad (21)$$

The derivative with respect to s, evaluated at $s = s_*$, will yield terms of the form $e^{s_* t}$ and $t\, e^{s_* t}$. It is obvious that s_* is a negative real number, so for any $n \geqslant 0$, $\lim_{t \to \infty} t^n e^{s_* t} = 0$. Just as before, $|V_S(t) - V_{\text{steady}}(t)| \to 0$ as $t \to \infty$. This proves (20) in the case where $P(s)/Q(s)$ has a double pole at $s = s_*$. $\qquad\square$

Now that we have obtained the steady-state solution using the Laplace transform, let us explain how the same result may be obtained much more expediently using the Fourier transform. Lemma 2 shows that to find the steady-state response of the system, it is sufficient to solve the problem with non-Heaviside right-hand side using the Fourier transform, ignoring initial conditions.

Lemma 2. *The steady-state solution of (17) is the function $W(t)$ that one obtains by solving*

$$\mathcal{L}W = L^{-1}V_{\text{in}}(t) \quad (22)$$

using the Fourier transform.

Proof. The only difference between (22) and (17) is the absence of the Heaviside term $H(t)$—in other words, we are now considering a system where the forcing term has been in existence 'from $t = -\infty$ until the present,' roughly speaking. We take the Fourier transform of both sides of (22) and obtain

$$[C_0(2\pi i\omega)^2 + R^{-1}(2\pi i\omega) + L^{-1}]\widehat{W}(\omega) = L^{-1} \sum_{m=1}^{M} \beta_m \delta(\omega - \alpha_m).$$

We solve for $\widehat{W}(\omega)$:

$$\widehat{W}(\omega) = L^{-1} \sum_{m=1}^{M} \frac{\beta_m \delta(\omega - \alpha_m)}{C_0(2\pi i\omega)^2 + R^{-1}(2\pi i\omega) + L^{-1}}.$$

Now inverting the Fourier transform, which is trivial because of the Dirac δ's on the right-hand side, we obtain $W(t) = V_{\text{steady}}(t)$, as desired.   □

Remark 1.   When we solve $\mathcal{L} f(t) = g(t)$, the solution $f(t)$ contains only those Fourier modes that were originally present in $g(t)$. No new Fourier modes are created. This is clear from the steady-state solutions derived in both lemmas 1 and 2.

Lemma 3 has to do with what happens in the system (12)–(13) when we start with $V_{\text{in}}(t)$ equal to a real-valued trigonometric function at a single frequency, which we call the fundamental mode. In this case, when k is odd, we find that $w_k(t)$ can consist only of even harmonics; likewise, when k is even, we find that $w_k(t)$ can consist only of odd harmonics. Most importantly for the results that we present in section 3, when k is even, $w_k(t)$ will contain some multiple of the fundamental mode.

Lemma 3.   *Suppose that* $V_{\text{in}}(t) = A\, e^{2\pi i \omega t} + \overline{A}\, e^{-2\pi i \omega t}$. *Then the solution of (12)–(13) can be written in the form*

$$w_{2l}(t) = \sum_{j=0}^{l} a_{2j+1}\, e^{2\pi i (2j+1)\omega t} + \overline{a_{2j+1}}\, e^{-2\pi i (2j+1)\omega t}, \tag{23a}$$

$$w_{2l+1}(t) = \sum_{j=1}^{l+1} b_{2j}\, e^{2\pi i (2j)\omega t} + \overline{b_{2j}}\, e^{-2\pi i (2j)\omega t}, \tag{23b}$$

where the a and b coefficients depend on l.

Proof.   Applying lemma 1 to the first equation (12), we find that
$$w_0(t) = B\, e^{2\pi i \omega t} + \overline{B}\, e^{-2\pi i \omega t}, \tag{24}$$
for an appropriate complex constant $B \sim A$. This implies that for $k = 1$, (13) is
$$\mathcal{L} w_1 = 8 C_1 \pi^2 \omega^2 [B^2\, e^{4\pi i \omega t} + \overline{B^2}\, e^{-4\pi i \omega t}].$$
By lemma 1, this implies that
$$w_1(t) = D\, e^{4\pi i \omega t} + \overline{D}\, e^{-4\pi i \omega t}, \tag{25}$$
again for an appropriate complex constant $D \sim A^2$. Our expressions for $w_0(t)$ and $w_1(t)$ verify (23) for $l = 0$. We now proceed inductively. Assume that (23) is true for $l = 0, 1, 2, \ldots, \Lambda$. We then use (13) to write

$$\mathcal{L} w_{2\Lambda+2} = -C_1 \frac{\mathrm{d}}{\mathrm{d}t} \sum_{n=0}^{2\Lambda+1} w_n \frac{\mathrm{d}}{\mathrm{d}t} w_{2\Lambda+1-n}$$
$$= -C_1 \frac{\mathrm{d}}{\mathrm{d}t} \left[\sum_{m=0}^{\Lambda} w_{2m} \frac{\mathrm{d}}{\mathrm{d}t} w_{2(\Lambda-m)+1} + \sum_{m=0}^{\Lambda} w_{2m+1} \frac{\mathrm{d}}{\mathrm{d}t} w_{2(\Lambda-m)} \right].$$

In the first sum on the right-hand side, each term in the sum is the product of an odd mode (from the even term w_{2m}) with an even mode (from the derivative of the odd term $w_{2(\Lambda-m)+1}$). Each term must therefore be an odd mode, so the first sum will be a sum of odd modes. The second sum must also be a sum of odd modes, by analogous reasoning. Writing this out, we obtain

$$\mathcal{L} w_{2\Lambda+2} = -C_1 4\pi i \omega \frac{\mathrm{d}}{\mathrm{d}t} \sum_{m=0}^{\Lambda} \sum_{j=0}^{m} \sum_{k=1}^{\Lambda-m+1} k a_{2j+1} b_{2k}\, e^{2\pi i (2j+2k+1)\omega t}$$
$$+ k \overline{a_{2j+1}} b_{2k}\, e^{-2\pi i (2j-2k+1)\omega t} + \text{c.c.}$$

In the above equation, 'c.c.' stands for the complex conjugate of the preceding terms. Because $(2j + 2k + 1)$ and $(2j - 2k + 1)$ are always odd, the right-hand side consists only of odd modes. The largest mode is the $(2\Lambda + 3)$th mode. Note also that when $k = 1$, $(2j - 2k + 1)$ will equal ± 1 when $j = 1$ or $j = 0$, so there will also be a contribution of $e^{\pm 2\pi i \omega t}$, also known as the fundamental mode. Therefore, we see that the equation for $w_{2\Lambda+2}$ can be written in the form

$$\mathcal{L}w_{2(\Lambda+1)} = \sum_{j=0}^{\Lambda+1} B_{2j+1}\, e^{2\pi i(2j+1)\omega t} + \overline{B_{2j+1}}\, e^{-2\pi i(2j+1)\omega t},$$

for suitable complex constants B_{2j+1}. Then by lemma 1, we have verified (23*a*) for $l = \Lambda + 1$.

Our next task is to verify (23*b*) for $l = \Lambda + 1$. We start with (13) and write

$$\mathcal{L}w_{2\Lambda+3} = -C_1 \frac{d}{dt} \sum_{n=0}^{2\Lambda+2} w_n \frac{d}{dt} w_{2\Lambda+2-n}$$

$$= -C_1 \frac{d}{dt}\left[\sum_{m=0}^{\Lambda+1} w_{2m} \frac{d}{dt} w_{2(\Lambda-m+1)} + \sum_{m=0}^{\Lambda} w_{2m+1} \frac{d}{dt} w_{2(\Lambda-m)+1} \right].$$

This time, the first sum on the right-hand side contains odd modes multiplied by odd modes, since both $2m$ and $2(\Lambda - m + 1)$ are always even. Similarly, the second sum on the right-hand side contains even modes multiplied by even modes, since both $(2m + 1)$ and $2(\Lambda - m) + 1$ are always odd. Therefore, the entire right-hand side consists of a sum of even modes—modes of the form $e^{\pm 2\pi i(2q)\omega t}$ for the integer values of q. Writing everything out, we will find that the largest mode is the $(2\Lambda + 4)$th mode. Therefore, we may write

$$\mathcal{L}w_{2(\Lambda+1)+1} = \sum_{j=0}^{\Lambda+2} D_{2j}\, e^{2\pi i(2j)\omega t} + \overline{D_{2j}}\, e^{-2\pi i(2j)\omega t},$$

for suitable complex constants D_{2j}. We apply lemma 1 one last time to conclude that (23*b*) is true for $l = \Lambda + 1$, finishing the induction step and the proof. □

At each order of ε, the function $w_k(t)$ is the steady-state solution of the damped, driven linear system (13). Therefore, we refer to the sum (11) as the steady-state solution of the damped, driven nonlinear system (4). Inspecting (11) and (24), we see that if $\varepsilon = 0$, i.e. if the capacitors do not depend on voltage, then the steady-state solution contains no harmonics other than the fundamental. In this case, the steady-state solution consists of $V(t) = w_0(t)$.

When $\varepsilon \neq 0$, i.e. when we switch on the nonlinearity in the system, the circuit transfers energy from the fundamental frequency (or first harmonic) of the input function into higher harmonics. As is evident from (11) and (23), at order ε^k, the solution $w_k(t)$ will contain a linear combination of harmonics all the way up to the $(k + 1)$st harmonic. Through this process, the period of $V(t)$ remains the same as the period of $V_{\text{in}}(t)$—both input and output signals have the period $T = 1/\omega$.

For the purposes of illustration, we have numerically integrated (1) with parameters $C_0 = C_1 = 1$, $\varepsilon = 0.1$, $L = 1$, $R = 3.281\,24$ and with input signal given by (14) with $A = 2.2$ and $\omega = 0.170\,988$. In the left panel of figure 3, we plot $(I(t), V(t))$ for $t = 0$ until $t = 20/\omega$. This phase portrait shows that the system starts at the origin and approaches a nonlinear oscillatory steady state (or limit cycle). In the right panel of figure 3, we have plotted in a dashed line the numerically obtained steady-state solution for $V(t)$. Superimposed on this dashed line is a solid line consisting of approximation (11) truncated at $k = 10$. The perturbative approximation deviates slightly from the numerical solution for those values of t, where the $(I(t), V(t))$ trajectory turns its sharpest corner, i.e. in the lower-left quadrant of
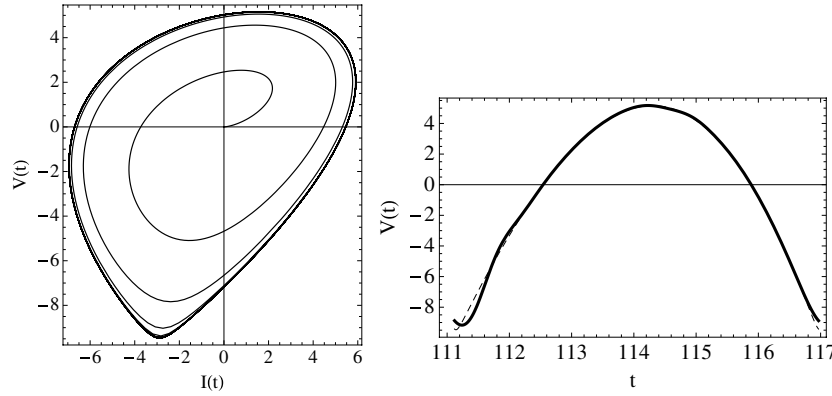
Figure 3. The left panel shows the phase trajectory $(I(t), V(t))$ obtained by numerically integrating (2) until the system has reached steady state. The right panel compares the numerically obtained steady-state solution (dashed line) with the perturbative approximation (11) truncated at $k = 10$. The only values of t for which the perturbative and numerical solutions differ are those for which the phase portrait exhibits the greatest local curvature.

the left panel of the figure. If we were to redo this comparison with, say, $A = 1.1$, then the nonlinear limit cycle would not be so sharply curved in the lower-left quadrant, and the perturbative and numerical approximations would be indistinguishable.

Remark 2. As described in the proof of lemma 3, the even numbered functions $w_{2k}(t)$ contain a linear combination of odd harmonics starting with the fundamental. Therefore, when $\varepsilon \neq 0$, the solution $V(t)$ at $(2k)$th order will contain a term of the form

$$\varepsilon^{2k}(c_{2k}A^{2k+1}\,e^{2\pi i\omega t} + \text{c.c.}),\tag{26}$$

for suitable complex constants c_{2k}. The power of A arises naturally from the quadratic nonlinearity on the right-hand side of (13).

Taken together, the results indicate that the response $V(t)$ of the system to the input function (14) will be smooth and periodic with period T. That is, with this choice of input function, the response $V(t)$ can be expanded in a real Fourier series:

$$V(t) = \sum_{k=0}^{\infty} \alpha_k \cos 2\pi k\omega t + \sum_{k=1}^{\infty} \beta_k \sin 2\pi k\omega t.\tag{27}$$

We do not insert this directly into (4) because it leads to unnecessary complications, and in the rest of the paper, we do not need expressions for the coefficients α_k and β_k. Using (3), we have

$$I(t) = C(V)\frac{\mathrm{d}V}{\mathrm{d}t} + \frac{1}{R}V.$$

We conclude that $I(t)$ is T-periodic and smooth, and we can therefore write

$$I(t) = \sum_{k=0}^{\infty} \gamma_k \cos 2\pi k\omega t + \sum_{k=1}^{\infty} \delta_k \sin 2\pi k\omega t.\tag{28}$$

3. Energy conservation and voltage boosting

Let us add $I(t)$ times (1*a*) to $V(t)$ times (3). The result is

$$LI\frac{dI}{dt} + V\frac{dQ}{dt} = IV_{in}(t) - \frac{V^2}{R}. \tag{29}$$

The magnetic energy stored in the inductor at time t equals

$$E_{ind}(t) = \tfrac{1}{2}LI(t)^2. \tag{30}$$

The electrical energy stored in the capacitor at time t equals

$$E_{cap}(t) = \int_0^{Q(V(t))} V(q)\,dq, \tag{31}$$

where $V(q)$ is the inverse function of $Q(v)$. This implies that

$$\frac{d}{dt}E_{cap}(t) = V(t)\frac{dQ}{dt} = VC(V)\frac{dV}{dt}.$$

Hence, we may rewrite the left-hand side of (29) as a total derivative and obtain

$$\frac{d}{dt}\left[E_{ind}(t) + E_{cap}(t)\right] = IV_{in}(t) - \frac{V^2}{R}.$$

Integrating both sides from $t = 0$ to $t = T$ yields

$$E_{ind}(t) + E_{cap}(t)|_{t=0}^{t=T} = \int_0^T IV_{in}(t) - \frac{V^2}{R}\,dt. \tag{32}$$

Now let us assume that the system is in steady state, so that $V(t)$ and $I(t)$ are given by (27) and (28). Then $V(t)$ and $I(t)$ are both T-periodic, which implies by (30) and (31) that $E_{ind}(t)$ and $E_{cap}(t)$ are both T-periodic. Therefore, the left-hand side of (32) vanishes and we are left with

$$\int_0^T I(t)V_{in}(t)\,dt = \frac{1}{R}\int_0^T V(t)^2\,dt. \tag{33}$$

This says that when the system has reached steady state and all signals are T-periodic, the energy dissipated through the resistor in one cycle must equal the energy pumped into the system through the driving function.

Now we assume that $V_{in}(t)$ is given by the real input function (14), and we substitute the Fourier series expansion for $I(t)$ given by (28). Using orthogonality of the Fourier basis functions, (33) becomes

$$\int_0^T V(t)^2\,dt = \|V\|_2^2 = \frac{R\delta_1 A}{2\omega}.$$

Substituting (14), (27) and (28) into (1*a*), we obtain $\alpha_0 = 0$ and $\delta_1 = -\alpha_1/(2\pi L\omega)$, which means that

$$\|V\|_2^2 = -\frac{RA\alpha_1}{(2\omega)^2\pi L}. \tag{34}$$

Now, by the results of section 2 and remark 2, we know that

$$\alpha_1 = \sum_{k=0}^{\infty} \varepsilon^{2k} A^{2k+1} q_{2k}, \tag{35}$$

where the coefficients q_{2k} are real. In words, q_{2k} is the coefficient of $A^{2k+1} \cos 2\pi \omega t$ in the solution $w_{2k}(t)$. For example, using the methods of the previous section, we can write (24) with

$$B = \frac{-\mathrm{i}A}{2(-4\pi^2\omega^2 C_0 + 2\pi \mathrm{i}\omega/R + 1/L)},$$

which implies that

$$w_0(t) = (2\,\mathrm{Re}\,B) \cos 2\pi \omega t - (2\,\mathrm{Im}\,B) \sin 2\pi \omega t,$$

so that

$$Aq_0 = 2\,\mathrm{Re}\,B = -\frac{2\pi \omega A/R}{(-4\pi^2\omega^2 C_0 + 1/L)^2 + 4\pi^2\omega^2/R^2}.$$

Note that when C_0, L, R and ω are positive, then $q_0 < 0$. Therefore, if we define

$$K = -\frac{Rq_0}{4\omega^2 \pi L},$$

then $K > 0$. Using (35), we obtain from (34) the result

$$\|V\|_2 = \sqrt{K}\,A \left(1 + \sum_{k=1}^{\infty} \varepsilon^{2k} A^{2k} \frac{q_{2k}}{q_0}\right)^{1/2}. \tag{36}$$

3.1. Effect of nonlinearity

When $\varepsilon = 0$, the system is linear and (36) reduces to

$$\|V\|_2 = \sqrt{K}\,A,$$

showing that the L^2 norm of the output signal depends linearly on the input amplitude. Since the L^2 norm of the input signal is in fact $A/\sqrt{2\omega}$, we could equally well say that the L^2 norm of the output depends linearly on the L^2 norm of the input.

However, when $\varepsilon \neq 0$, the system is nonlinear and we can see from (36) that the L^2 norm of the output signal depends *nonlinearly* on the input amplitude A. If all the ratios q_{2k}/q_0 are positive, we can be certain that the quantity on the right-hand side of (36) will grow superlinearly for all A. However, superlinear growth on some interval, $A \in [0, A_{\max}]$, is possible when, say, $q_2/q_0 > 0$ and $q_4/q_0 > 0$ but $q_{2k}/q_0 < 0$ for $k \geqslant 3$. We examine this issue in section 3.3 below.

3.2. Relationship with L^∞ norm

Unfortunately, there appears to be no way to use Fourier coefficients to easily compute the L^∞ norm of $V(t)$. However, we can use the trivial upper bound

$$\int_0^T V(t)^2 \, \mathrm{d}t \leqslant T \|V\|_\infty^2$$

together with $T = 1/\omega$ to derive

$$\|V\|_\infty \geqslant \sqrt{\tilde{K}}\,A \left(1 + \sum_{k=1}^{\infty} \varepsilon^{2k} A^{2k} \frac{q_{2k}}{q_0}\right)^{1/2}, \tag{37}$$

where

$$\tilde{K} = \omega K = -\frac{Rq_0}{4\omega \pi L}.$$

When $\varepsilon = 0$, we know that the exact steady-state solution will be of the form $V(t) = \alpha_1 \cos 2\pi \omega t + \beta_1 \sin 2\pi \omega t$, so (36) reduces to

$$\frac{1}{\sqrt{2\omega}}\sqrt{\alpha_1^2 + \beta_1^2} = \sqrt{K}A.$$

Of course, for this exact solution, we know $\|V\|_\infty = \sqrt{\alpha_1^2 + \beta_1^2}$, so we have that

$$\|V\|_\infty = \sqrt{2\tilde{K}}A.$$

In other words, when $\varepsilon = 0$, the lower bound (37) is not sharp—to make it so, we would have to multiply the right-hand side of (37) by $\sqrt{2}$. This leads to the following *performance goal*: in order for the nonlinear system to have a steady-state output whose L^∞ norm obeys (37) *and exceeds* the L^∞ norm of the steady-state output for the corresponding linear system, the L^∞ norm of the nonlinear signal should obey

$$\|V\|_\infty \geqslant \sqrt{2\tilde{K}}A\left(1 + \sum_{k=1}^\infty \varepsilon^{2k}A^{2k}\frac{q_{2k}}{q_0}\right)^{1/2}. \tag{38}$$

Of course, unlike (37), the upper bound (38) will not be true for all choices of circuit parameters. We shall compare both lower bounds (37) and (38) against numerical simulations in section 3.4.

3.3. The coefficients q_{2k}/q_0

The proofs of lemmas 2 and 3 give an algorithmic procedure that can be used to iteratively solve the system (12)–(13). Implementing this procedure in Mathematica, we generated symbolic expressions for $w_0(t), w_1(t), \ldots, w_{10}(t)$, from which we can extract q_{2k} as the coefficient of $A^{2k+1}\cos 2\pi \omega t$ in $w_{2k}(t)$. In general, q_{2k} will depend on the parameters C_0, C_1, L, R and ω. Let us record here the value of one of the ratios we calculated:

$$\frac{q_2}{q_0} = \frac{32\pi^4 a^2 C_1^2 L^2 R^4 \omega^4\left(40\pi^4 C_0^2 L^2 R^2 \omega^4 - 2\pi^2 L\omega^2(7C_0R^2 + L) + R^2\right)}{(R^2(1 - 16\pi^2 C_0 L\omega^2)^2 + 16\pi^2 L^2\omega^2)(R^2(1 - 4\pi^2 C_0 L\omega^2)^2 + 4\pi^2 L^2\omega^2)^2}. \tag{39}$$

For reasons of space, we omit the algebraic expressions of the other ratios, q_{2k}/q_0 for $k = 2, 3, 4, 5$.

Before doing any further analysis, let us fix $L = C_0 = C_1 = 1$ and examine the R- and ω-dependence of the ratios q_{2k}/q_0 for $k = 1, 2, 3, 4$. We present the four contour plots in figure 4, each plotted for $(R, \omega) \in [0, 2] \times [0, 2]$. The areas shaded in gray are regions of (R, ω) parameter space in which the corresponding ratio is negative. The white areas with no shading represent regions of parameter space in which the corresponding ratio is positive.

For each of the four contour plots, we have examined what happens for larger values of R and ω than those shown here. In summary, as we follow the plots for $R > 2$, we find that the gray bands extend to the right indefinitely; however, the heights of these gray bands do not grow. When we follow the plots for $\omega > 2$, we find that the large white region continues indefinitely. However, for each of the four plots, in the large white expanse we find that the ratios are nearly constant, positive and small. The only region of parameter space in which we can find large variations in the ratios are immediately above and below the gray bands—see the contour lines that are in the white regions of each of the four plots.

Of course, the only reason that we are interested in those regions where the ratios q_{2k}/q_0 are positive is because we are mainly interested in the possibility that (36) gives us superlinear
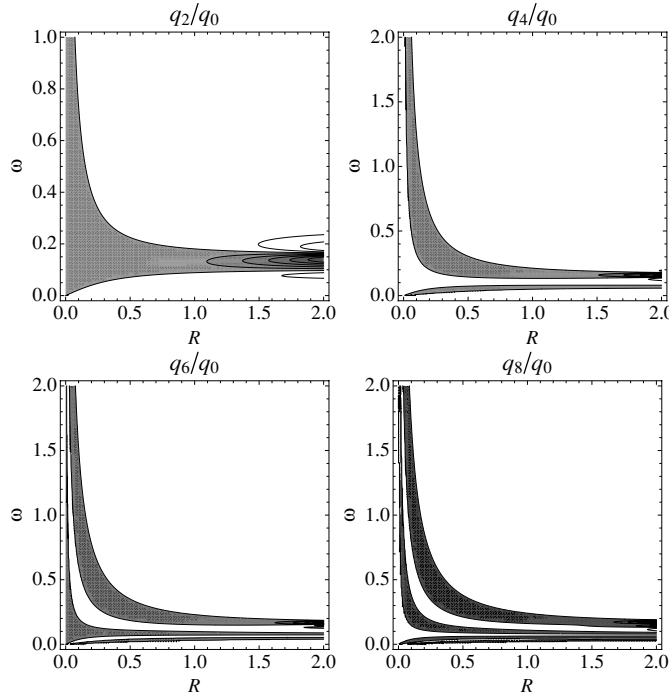
Figure 4. Each panel shows a contour plot for the corresponding ratio q_{2k}/q_0, for $k = 1, 2, 3, 4$. The white areas with no shading represent regions of parameter space in which the corresponding ratio is positive. The areas shaded in gray/black are regions of (R, ω) parameter space in which the corresponding ratio is negative. Here, we have fixed the parameters $L = C_0 = C_1 = 1$.

dependence of $\|V\|_2$ on A. As it turns out, we do not need *all* of the ratios q_{2k}/q_0 to be positive to guarantee this superlinear dependence for $A \in [0, A_{\max}]$ for some $A_{\max} > 0$.

Consider, for example, the circuit with the parameters $C_0 = C_1 = 1$, $\varepsilon = 0.1$, $L = 1$ and $R = \sqrt{10}$. Suppose the input signal has the frequency $\omega = 0.176\,598$. Then, we can calculate the values of the following ratios:

$$\frac{q_2}{q_0} = 0.025\,6221, \qquad \frac{q_4}{q_0} = 0.001\,017\,09, \qquad \frac{q_6}{q_0} = 0.000\,033\,7574, \qquad (40a)$$

$$\frac{q_8}{q_0} = -4.103\,03 \times 10^{-7}, \qquad \frac{q_{10}}{q_0} = -2.952\,98 \times 10^{-7}. \qquad (40b)$$

Though only the first three ratios are positive, this is enough to give us superlinear growth on the right-hand side of (36) for $A \in [0, 2]$. To see this, we plot the relative percentage boost in two-norm enjoyed by the nonlinear system over the corresponding linear system (i.e. the circuit with precisely the same parameters as given above, except that $\varepsilon = 0$):

$$P = \frac{\|V^{\text{nonlinear}}\|_2 - \|V^{\text{linear}}\|_2}{\|V^{\text{linear}}\|_2} \times 100 \approx \left[\left(1 + \sum_{k=1}^{5} \varepsilon^{2k} A^{2k} \frac{q_{2k}}{q_0}\right)^{1/2} - 1\right] 100, \qquad (41)$$

where the only reason for the approximation sign is that we have truncated the infinite sum on the right-hand side of (36) at $k = 5$, or tenth order in ε. The plot of P as a function of A, with the ratios given in (40), is shown in the left panel of figure 5. The plot clearly
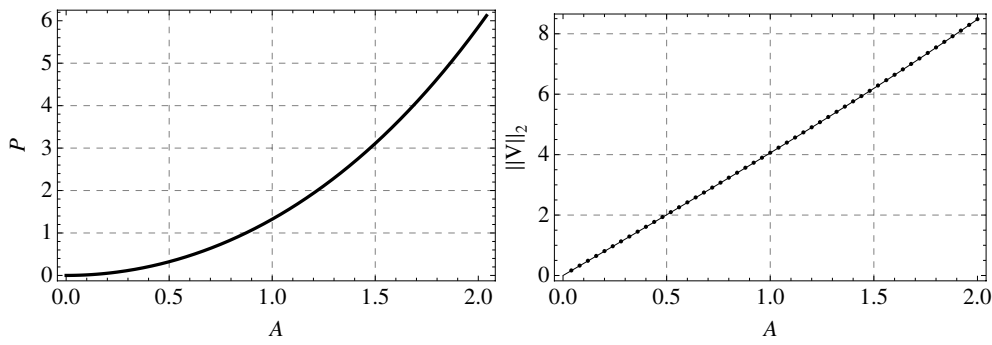
Figure 5. On the left, we plot the percentage boost P caused by nonlinearity—defined in (41)—as a function of input amplitude A. On the right, we plot the L^2 norm of the steady-state output signal, $\|V\|_2$, as a function of input amplitude A—the values indicated by circles were generated by numerically integrating Kirchhoff's laws (2) until they reached steady state and then computing $\|V\|_2$ over one period, while the line sitting behind the circles is a plot of the right-hand side of (36), truncated at $k = 5$. All plots are for a circuit with the parameters $C_0 = C_1 = 1$, $L = 1$, $R = \sqrt{10}$ and $\omega = 0.176\,598$. Nonlinearity was introduced by setting $\varepsilon = 0.1$; for the corresponding linear circuit, we set $\varepsilon = 0$.

shows that nonlinearity causes a boost in the two-norm of the steady-state output signal, and that this boost approaches 6% when the input amplitude reaches $A = 2$—in other words, the right-hand side of (36) depends superlinearly on A even though not all the ratios in (40) are positive.

   We have also plotted in the right panel of figure 5 the results of a numerical study. In this numerical study, we chose 50 equispaced values of A from $A = 0.04$ to $A = 2.00$. For each value of A, keeping the other parameters fixed ($C_0 = C_1 = 1$, $\varepsilon = 0.1$, $L = 1$, $R = \sqrt{10}$, $\omega = 0.176\,598$), we numerically integrated Kirchhoff's laws (1) until the solution reached steady state, and we then used the numerical solution to calculate $\|V\|_2$. What the right panel of figure 5 shows is that the numerically computed values of $\|V\|_2$ agree very closely with the right-hand side of (36). This verifies that truncating the expansion at $k = 5$, or, equivalently at tenth order in ε, yields an accurate measure of the L^2 norm of the steady-state output signal.

   For $|A| \gg 2$, our capacitor model becomes unphysical. A real voltage-dependent capacitor will saturate at voltages that are large in absolute value. Model (5) does not saturate, and hence is valid only for voltages that are not large in absolute value.

3.4. Numerical results on the L^∞ norm

As we mentioned before, computing a perturbative approximation to the L^∞ norm of the steady-state output is not a simple task. In figure 6, we compare the bounds (37) and (38) against numerical results.

   In the left panel of figure 6, we use the same circuit as in previous examples; the parameters are $C_0 = C_1 = 1$, $\varepsilon = 0.1$, $L = 1$, $R = \sqrt{10}$ and $\omega = 0.176\,598$. In this case, for each value of A, we numerically solve Kirchhoff's laws (1) until the solution reaches steady state and then compute the L^∞ norm of the numerical solution. The numerical results are plotted using small circles. One can see that the numerical values for $\|V\|_\infty$ do obey the rigorously derived upper bound (37), which is plotted as the solid curve with *smaller* slope. However, the numerical values for $\|V\|_\infty$ do not obey the performance goal (38), which is plotted as the solid curve with *larger* slope. In this case, if one's goal is to produce a steady-state output
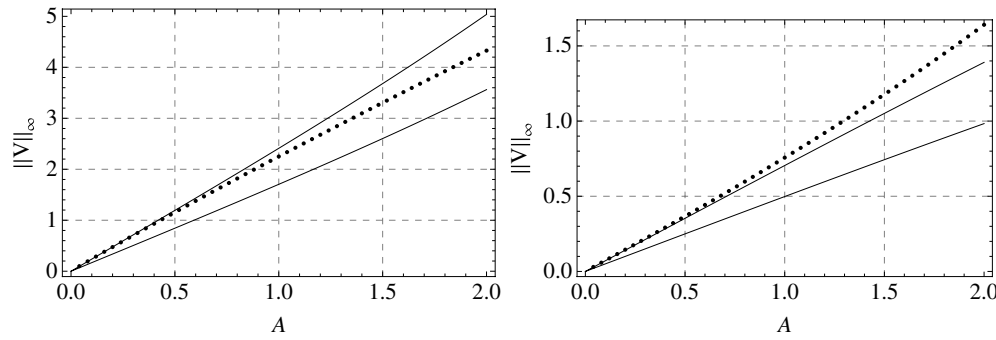
Figure 6. These plots compare the L^∞ bounds (37) and (38) against numerical results. In both plots, the straight, solid line with smaller (respectively, larger) slope is given by the right-hand side of (37) (respectively, (38)). Each small circle is the result of numerically integrating Kirchhoff's laws (2) until the solution reached steady state, and then using the numerically computed solution to calculate $\|V\|_\infty$. In the left panel, the circuit parameters were $C_0 = C_1 = 1$, $\varepsilon = 0.1$, $L = 1$, $R = \sqrt{10}$ and $\omega = 0.176\,598$. In the right panel, the circuit parameters were $C_0 = 1$, $C_1 = -0.5$, $\varepsilon = 1$, $L = 0.5$, $R = 0.5$ and $\omega = \sqrt{2}/(2\pi)$. Unlike in the left panel, the L^∞ norms in the right panel do satisfy the performance goal (38), indicating that this circuit has a genuine advantage over the corresponding linear circuit (with $\varepsilon = 0$), if the goal is to produce the steady-state output with the largest L^∞ norm.

signal $V(t)$ that has the largest possible L^∞ norm, one would do better using the linear $\varepsilon = 0$ circuit.

In the right panel of figure 6, we use a different nonlinear circuit; the parameters are now $C_0 = 1$, $C_1 = -0.5$, $\varepsilon = 1$, $L = 0.5$, $R = 0.5$ and $\omega = \sqrt{2}/(2\pi)$. We carry out the same numerical procedure as described in the previous paragraph and plot the numerically computed values of $\|V\|_\infty$ using small circles. This time, the numerical values for $\|V\|_\infty$ obey not only the rigorous lower bound (37), but also the performance goal (38). This shows that there are indeed circuits whose steady-state outputs obey (38), and that this performance goal could be used as a constraint in an algorithm that uses optimization to find the nonlinear circuit that exhibits the greatest relative boost in $\|V\|_\infty$ over the corresponding linear system.

4. Conclusion

In this work, we have analyzed the steady-state oscillations of a damped, driven nonlinear *LRC* oscillator. In the perturbative regime where (11) converges, we find only harmonic oscillations at the same period as the input forcing.

We fully expect that when the driving amplitude A is sufficiently large, the perturbative expansion (11) will break down. This will lead to possible subharmonic oscillations and oscillations with other periods, which we shall analyze in future work, using a capacitor model that saturates at very high and very low voltages.

The beauty of the perturbative approach is that we can combine it with an argument about steady-state energy conservation to determine the L^2 norm of the output signal. We showed that there is a large region of parameter space where the L^2 norm of the nonlinear system's output signal exceeds the L^2 norm of the output signal for the corresponding linear system.

Because we have an algorithm for determining symbolic expressions of the coefficients q_{2k}/q_0 that play a role in the nonlinear signal's L^2 norm—and possibly in the L^∞ norm as well, our analysis enables one to use optimization methods to design systems where nonlinearity causes the maximum possible gain relative to the corresponding linear system.

This work provides an analytical derivation of a property that has only been noted experimentally and numerically in our prior work [BA08, LPL+10]. In the experimentally described circuits, the coefficients C_0, C_1 and ε are chosen so that the ratios described above, q_{2k}/q_0, do indeed turn out to be positive. The above derivations provide a mathematical justification for why we have observed a nonlinear dependence of the output two-norm and amplitude on the input amplitude.

Finally, in future work, we shall apply these techniques to networks of nonlinear oscillators. We hope to show that even if each individual *LRC* oscillator provides only a small boost, the aggregate effect of a large number of oscillators could be quite large, depending on the network topology and other design factors.

Acknowledgments

References

[ABHM06] Afshari E, Bhat H S, Hajimiri A and Marsden J E 2006 Extremely wideband signal shaping using one- and two-dimensional nonuniform nonlinear transmission lines *J. Appl. Phys.* **99** 054901
[BA08] Bhat H S and Afshari E 2008 Nonlinear constructive interference in electrical lattices *Phys. Rev. E* **77** 066602
[BW06] Butt I A and Wattis J A D 2006 Discrete breathers in a two-dimensional Fermi–Pasta–Ulam lattice *J. Phys. A: Math. Gen.* **39** 7283–98
[BW07] Butt I A and Wattis J A D 2007 Discrete breathers in a two-dimensional hexagonal Fermi–Pasta–Ulam lattice *J. Phys. A: Math. Theor.* **40** 1239–64
[Hay85] Hayashi C 1985 *Nonlinear Oscillations in Physical Systems* (Princeton, NJ: Princeton University Press)
[Hu06] Hu H 2006 Solution of a quadratic nonlinear oscillator by the method of harmonic balance *J. Sound Vib.* **293** 462–8
[LPL+10] Lilis G N, Park J, Lee W, Li G, Bhat H S and Afshari E 2010 Harmonic generation using nonlinear LC lattices *IEEE Trans. Micro. Theory Tech.* accepted
[Mic04] Mickens R E 2004 Quadratic non-linear oscillators *J. Sound Vib.* **270** 427–32
[NM79] Nayfeh A H and Mook D T 1979 *Nonlinear Oscillations* (New York: Wiley Interscience)
[OPS80] Ostrovskii L A, Papko V V and Stepanyants Yu A 1980 Solitons and nonlinear resonance in two-dimensional lattices *Zh. Eksp. Teor. Fiz.* **78** 831–41 (*Sov. Phys.—JETP* **51** 417 (1980))
[Ste81] Stepanyants Yu A 1981 Experimental investigation of cylindrically diverging solitons in an electric lattice *Wave Motion* **3** 335–41
[Ste83] Stepanyants Yu A 1983 Experimental study of 'Cerenkov' radiation from solitons in two-dimensional LC-lattices *Radiophys. Quantum Electron.* **26** 601–7
[VMM+96] Vakakis A F, Manevitch L I, Mikhlin Y V, Pilipchuk V N and Zevin A Z 1996 *Normal Modes and Localization in Nonlinear Systems* (New York: Wiley)